

Electrical Resistivity Characterization of a Reclaimed Gold Mine to Delineate Acid Rock Drainage Pathways

Dale F. Rucker · Danney R. Glaser ·
Tom Osborne · William C. Maehl

Received: 16 February 2009 / Accepted: 16 April 2009
© Springer-Verlag 2009

Abstract An electrical resistivity survey was completed at the Landusky mine. The survey consisted of 15 lines on the surface of the reclaimed Surprise pit, Queen Rose pit, and the region immediately south of Swift Gulch. Additionally, wells and seeps were used by energizing electrodes in direct contact with ground water to increase the sensitivity of the resistivity method at depth. The survey was conducted to locate potential acid rock drainage pathways that are contaminating Swift Gulch. The results showed that the lowest resistivity values were coincident with the Queen Rose pit. Furthermore, the low resistivity feature appeared to trend northeast along a known fault, consistent with the geologic understanding of the site. A scatter plot of resistivity values versus total dissolved solids (TDS) showed a strong correlation ($R^2 = 0.85$). A linear regression model suggests TDS at the lowest resistivity region to be approximately 2.5 times greater than that measured in ground water wells.

Keywords Geophysics · Characterization · Reclamation · Acid rock drainage · Mining · Electrical resistivity

Introduction

The contribution of a mining project to the local and national economy, as well as its external societal impacts is a valuable resource (Damigos 2006). However, the cost associated with reclamation, mitigation, and monitoring of improperly controlled and abandoned mines can be staggering. Warhurst and Mitchell (2000), for example, placed the to-date costs of environmental restoration (including water treatment, pit capping, adit plugging, and regrading) of the Summitville gold mine in Colorado in excess of \$150 million. Although the mobilization of cyanide from past leaching activities caught the attention of state and federal regulatory agencies, it is the acid rock drainage (ARD) that poses the most significant long-term environmental risks. The Zortman and Landusky open pit gold mines of north-central Montana are also subject to high reclamation and water treatment costs from ARD. Cost estimates over the life cycle of these two closely spaced mines include posted reclamation and water treatment bonds of \$68 million, an additional \$12 million in state and federal funding, and \$17 million needed from yet undetermined sources (Shaw et al. 2001; Spectrum Engineering 2009).

Unfortunately, ARD is a common environmental problem at thousands of abandoned base and precious metal mine sites in the Rocky Mountains and western United States (Hazen et al. 2002). Whether natural or anthropogenically caused, ARD poses problems for local watersheds, including streams (Bird 2003; Parker et al. 2007), soil (Da Silva et al. 2005; Finlayson et al. 2000; El Khalil et al. 2008; Liu et al. 2003), ground water (Brown et al. 1998; Johnson 2007; Malmstrom et al. 2008), and aquatic life (Fischer and Sexauer 2002; Mian and Yanful 2003; Passariello et al. 2002; Saiki et al. 2001; Salomons 1995).

D. F. Rucker (✉) · D. R. Glaser
hydroGEOPHYSICS, Inc., 2302 N Forbes Blvd,
Tucson, AZ 85745, USA
e-mail: drucker@hgiworld.com

T. Osborne
HydroSolutions, Inc., 1537 Avenue D, Suite 340,
Billings, MT 59102, USA

W. C. Maehl
Spectrum Engineering, Inc., 1413 North 4th Avenue,
Billings, MT 59101, USA

The most severe environmental problems typically stem from low pH water and the mobilization of heavy metals from pits, leach pads, and waste rock piles. Although iron and aluminum typically are the main dissolved species in ARD, others such as cadmium, lead, zinc, and copper may also be present.

Once offsite, the ARD may require expensive treatment options to mitigate against further degradation of the watershed. These options are limited to the invasive capture and control of ground water, through pump-and-treat, reactive barriers, or funnel and gate systems (Bayer and Finkel 2006). Proper characterization is necessary to understand the source and direction of ARD. Geophysical characterization, and in particular electrical resistivity, is an attractive option to begin understanding the flow of ARD based on price and coverage. A resistivity survey will generally be more cost effective than drilling a large number of wells, and the method can be used to assure that any new wells are sited correctly.

We present the results of an electrical resistivity survey conducted at the Landusky gold mine. Electrical resistivity was chosen based on the method's ability to discriminate water laden with ionic constituents, such as ARD. The goal of the survey was to help build a conceptual model of the ARD transport from the mine to Swift Gulch, a perennial stream located immediately north of the site. The mine consists of five pits, several leach pads and waste rock piles, and containment ponds. The survey focused on the northern two pits, namely the Surprise and Queen Rose pits, which are in closest proximity to the gulch and connected through a steep hydraulic gradient. A few have used electrical resistivity to map contamination from mine waste sites (Ebraheem et al. 1990; Merkel 1972; Yuval and Oldenburg 1996; Spindler and Olyphant 2004), but they have been limited to small coverage areas or one-dimensional analyses. The work completed at Landusky includes a three-dimensional analysis over 21 ha. Taken together, the size, data density, and dimensionality of this work provides a more complete picture of potential ARD contamination resulting from mining activities.

Study Site

History

The Landusky mine and the nearby Zortman mine (5 km northeast of Landusky) are located in Phillips County Montana, in a historic mining district. Figure 1 shows the site location. A gold rush occurred after gold was discovered in Alder Gulch on July 3, 1884. As a result, part of the Little Rocky Mountains was acquired in the Grinnell Treaty in 1895, a purchase by the United States from the

Fort Belknap reservation. Underground mining proceeded intermittently at both the Landusky and Zortman areas until World War II.

After that, very little mining occurred until the mid-1970s, when Pegasus Gold Corporation identified a viable low-grade gold and silver deposit. An environmental impact analysis completed in 1979 led to the issuance of operating permits for two open pit mining and heap leaching operations that same year. Prior to 1979, no open pit mining occurred in this area.

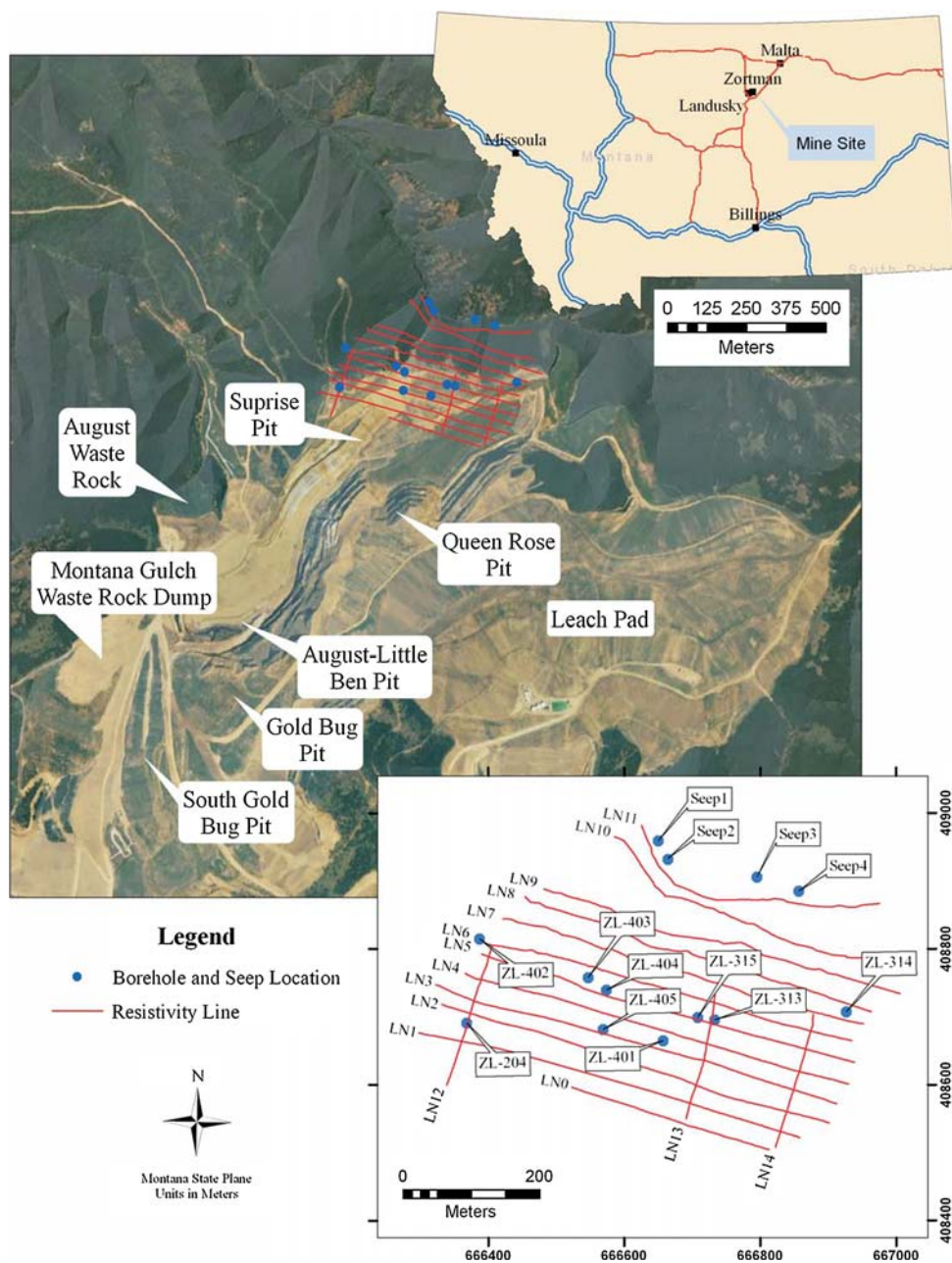
Pegasus Gold Corporation commenced voluntary chapter 11 bankruptcy proceedings on January 16, 1998. Since that time, the Bureau of Land Management (BLM) and Montana Department of Environmental Quality (DEQ) have worked together to implement closure of the mine using reclamation and water treatment bonds along with other funding sources. The Montana DEQ and the BLM now oversees the reclamation of the mine through BLM's CERCLA jurisdiction.

Geology

The Little Rocky Mountains, host to the Landusky mine, occupy an area of about 250 km² and rise up to 1,000 m above the surrounding plain (Wilson and Kyser 1988). The mountains are part of the larger Central Montana Alkalic Province that extends south-southeast from the Canadian border to Yellowstone National Park. The Little Rocky Mountains were formed when a calc-alkalic to alkalic magma of early Tertiary age penetrated through the Precambrian basement and into the Paleozoic and Mesozoic sedimentary rocks (Hastings 1988). The sedimentary rocks originated largely under marine conditions and consist primarily of limestone, dolomite, shale, sandstone, and conglomerates (Knechtel 1959).

The Landusky silver-gold ore body is unusual in that the gold is hosted in the fracture systems of the intrusive rocks, similar to that of base metal deposits. The structurally controlled epithermal bodies can occur as narrow veins and high-grade native gold to oxidized low-grade stockworks, breccias, and intensively fractured sheeted zones near the surface (Hastings 1988). The low-grade material appears in a large shear zone bounded by the Niseka-August fault in the north and Gold Bug fault on the south. This material was part of the open pit mining operation that formed the Surprise and Queen Rose pits. The Niseka-August and Gold Bug faults are fairly continuous along strike, which trends to the northeast. The faults are high angle reverse faults that dip towards the northwest (Richardson 1973). Within the shear zone, there are at least four sympathetic subparallel veins, shown in Fig. 2, with an average dip between 75 and 80° northwest (Richardson 1973).

Fig. 1 Location of the Landusky study site



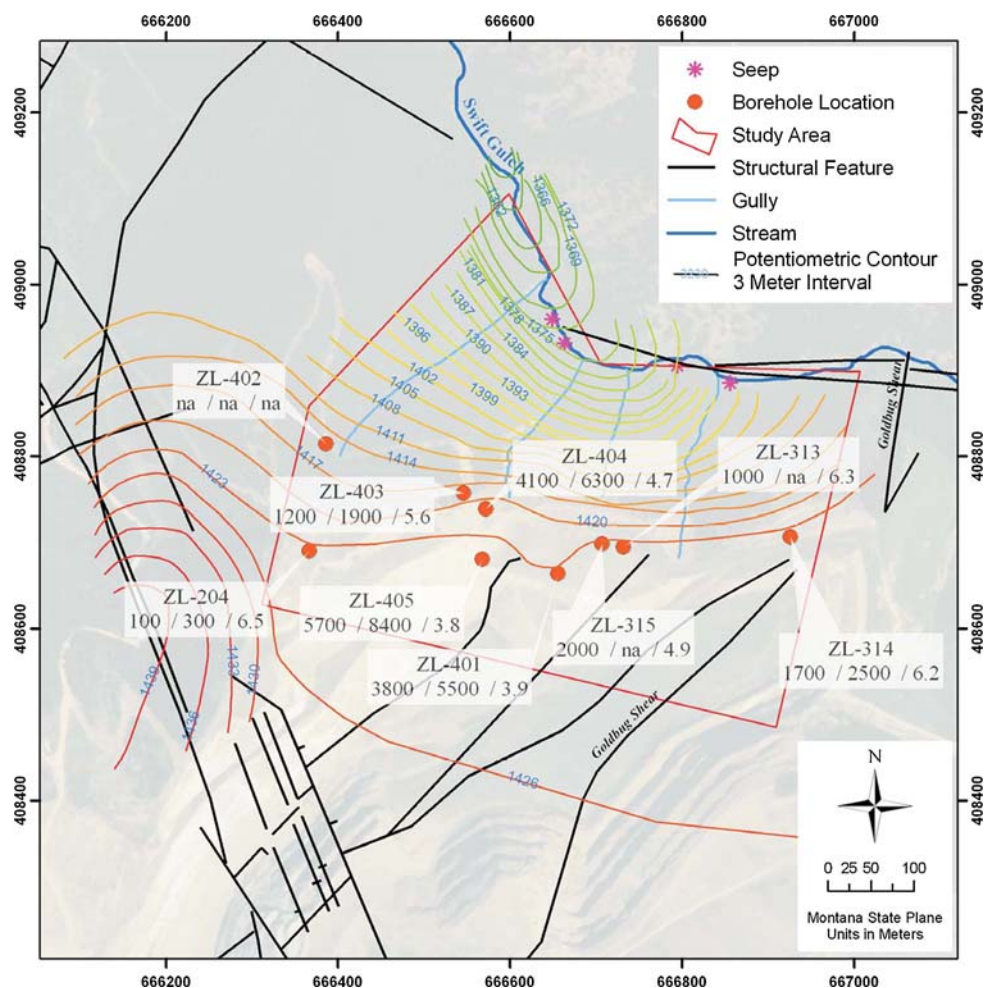
The Tertiary intrusion consists mainly of porphyritic syenite, quartz monzonite, and other undifferentiated intrusive materials. The degree of oxidation was an important factor in pit mining and leaching of the low grade stockworks (Hastings 1988). The degree of oxidation decreased with depth, with the oxide/sulfide boundary extending down to 150 m along the mineralized fault zones. However, pit blasting fractured the sulfidic ore, exposing pyrite to oxidation, thus lowering the pH of the infiltrating water. During post-bankruptcy geochemical monitoring, Shaw et al. (2000) showed that water samples from the pit generally had lower pH readings than the leach pads, waste rock, and stockpiles. The low pH likely results

from the oxidation of pyrite within the pit, as well as that naturally occurring within the host rock.

Reclamation

After the bankruptcy proceedings in January 1998, DEQ began administering reclamation and water treatment. Reclamation activities included filling the pits with relatively inert waste rock, regrading and reseeding the leach pads, and installing water treatment plants to treat nitrates, cyanide, and selenium from the leach pad waters. The Queen Rose and Surprise pit floors were covered with a bentonite liner, and limestone was also placed against the

Fig. 2 Geologic and hydrogeologic information of the Landusky Mine area, showing major faults and fractures, potentiometric surface, and ground water quality data. The ground water quality data for the wells are sulfate (mg/L), total dissolved solids (mg/L), and pH



Surprise pit highwalls. The pits were covered with low permeability material and revegetated to prevent meteoric water from infiltrating.

The effects of the ARD can be seen in Fig. 2. Several wells are being used as ground water sampling locations north of the pits, with the 300 series installed long before the 400 series wells. The 400 series wells were installed specifically along the north end of the pits above Swift Gulch in an attempt to locate the hydraulic pathways that are associated with the northeast trending shear zones. These shear zones act as conduits for acidic ground water to move from the mine to Swift Gulch, as demonstrated by tracer testing. Tracer concentrations in surface water and springs in Swift Gulch were monitored for approximately 2 years with results showing a hydraulic connectivity between the mine and gulch (Osborne et al. 2006).

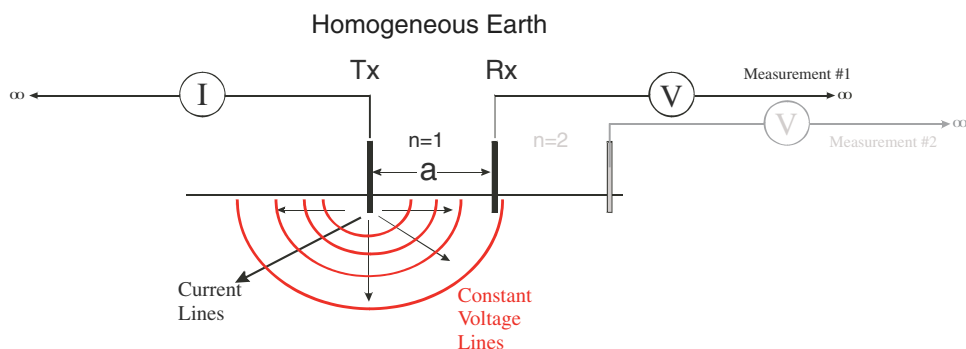
The ground water quality data of Fig. 2 show a general trend of increasing quality away from the mine. The water table, also presented in Fig. 2, shows a strong hydraulic gradient between the mine and gulch, indicating a potentially high velocity of ARD away from the mine. The pH

appears particularly low near the pits with values of 3.8 and 3.9 in wells ZL-405 and ZL-401, respectively.

Description of Electrical Resistivity

Electrical resistivity is a volumetric property that describes the resistance of electrical current flow within a medium, and can be used to remotely observe changes in hydrogeological properties or extend “ground truth” information about geochemical conditions based on borehole data. Direct electrical current is propagated in rocks and minerals by electrolytic and electronic conduction (Telford et al. 1990). Porous media can pass current through ions within the open framework of the pore space by way of electrolytic conduction, which relies on the dissociation of ionic species. Here, the conduction varies with the mobility, concentration, and degree of dissociation. By contrast, electronic conduction occurs in metallic-luster sulfide minerals, such as that found in precious metal mines, where free electrons are available. Rocks and non-metallic

Fig. 3 Schematic of the pole–pole array. Tx = transmitter, Rx = receiver



minerals have extremely high resistivity (low conductivity) and direct current transmission through this material is difficult. Electrolytic conduction is relatively slow with respect to electronic conduction due to mass transfer rate limiting processes.

The resistivity method employs electric current that is injected into the earth through one pair of electrodes (transmitting dipole) and measures the resultant electric field potential across another pair of electrodes (receiving dipole). The electric current is generated by battery or motor-generator driven equipment. Field data are acquired using a multi-electrode array along linear transects. A multi-electrode array enables rapid data acquisition over a large area with minimal reconfiguration of equipment. Common array configurations include Wenner, Schlumberger, and dipole–dipole arrays.

An alternative to the basic two-dipole, four-electrode array is the two-electrode pole–pole array. For the pole–pole array, one electrode from each of the current and potential dipoles is fixed effectively at infinity, while the other current and potential electrodes act as “rover” electrodes within the survey transect. Figure 3 shows a schematic of the pole–pole array and effects of a heterogeneous block on the voltage. Practically, the infinite electrodes are spaced approximately 5–10 times the distance of the furthest separation of the rover electrodes, which can be up to 300 m apart for a near surface geophysical survey. The pole–pole array provides higher data density, increased signal to noise ratio, and requires less transmitted energy (Robain et al. 1999). Roy and Apparao (1971) discuss the superiority of the pole–pole method when conducting shallow surveys. Additionally, in some conductive environments, where potential gradients are low, one may be forced to use the pole–pole array to simply measure a signal above the noise level of the data acquisition instrument.

Estimating resistivity is not a direct process (Rucker and Fink 2007). When current (I) is applied and voltage (V) measured, Ohms law is assumed and resistance is calculated. The ratio of the transmitted current and observed potential is called the transfer resistance (R). Resistivity

and resistance are then related through a geometric factor over which the measurement is made. The simplest example is a solid cylinder with a cross sectional area of A and length, L:

$$\rho = R \frac{A}{L} \tag{1}$$

In such cases where the actual volume involved in the measurement is known, the result is called the “true” resistivity and is considered to be a physical property of that material. However, field measurements involve an unknown volume of earth. Consequently, resistivity calculations are based on the hypothetical response for the given electrode geometry over a homogeneous, isotropic, half-space. This result is what is termed “apparent” resistivity, which is calculated for the pole–pole array by:

$$\rho_a = 2\pi \frac{V}{I} (n * a) \tag{2}$$

where n and a are defined in Fig. 3.

An estimate of the true resistivity is calculated through an inverse procedure. Inversion involves calculating the resistivities of the subsurface that would give rise to the measured apparent resistivity, according to the governing partial differential equation:

$$\frac{\partial}{\partial x} \left(\frac{1}{\rho} \frac{\partial V}{\partial x} \right) + \frac{\partial}{\partial y} \left(\frac{1}{\rho} \frac{\partial V}{\partial y} \right) + \frac{\partial}{\partial z} \left(\frac{1}{\rho} \frac{\partial V}{\partial z} \right) + I = 0 \tag{3}$$

Notice Eq. 2 is at steady state, i.e. the potential field is established instantaneously. The objective of the inversion is to minimize the difference between the modeled and measured apparent resistivity, usually in a least squares sense. The general form of the objective function for the resistivity inversion is primarily based on weighted least squares:

$$(d_{\text{calc}} - d_{\text{meas}})^T W_d (d_{\text{calc}} - d_{\text{meas}}) \tag{4}$$

where d_{calc} is the calculated voltage data from the numerical modeling at coincident locations with d_{meas} , which represents the measured voltage. W_d is a weighted

function based on the measurement errors and is equal to the inverse of the error covariance matrix. The objective function has been updated many times to include other terms, such as smooth model constraints (i.e., a smooth model based on minimizing the second spatial derivative of the resistivity). For the inverse models completed on the Landusky data, the smooth model criterion was invoked and the final objective function for smooth model inversion is represented by:

$$S(m) = (d_{\text{calc}} - d_{\text{meas}})^T W_d (d_{\text{calc}} - d_{\text{meas}}) + \lambda (m - m_0)^T R (m - m_0) \quad (5)$$

where the second term represents model smoothness, λ is the dampening factor, m is the model parameter of resistivity at every cell, m_0 is the a priori information and/or initial starting guess, and R is the difference operator for estimating model smoothness.

In general, the automated inversion routine for inverse modeling proceeds as follows:

1. The Earth's voltage data has been measured and is discretized into grid nodes using a finite difference or finite element mesh. The meshing parameters depend on electrode spacing. The inversion will set out to estimate the true resistivity at every grid node.
2. An initial estimate of the subsurface properties is made based on the literal translation of the pseudo-section to a true resistivity, a constant value, or some other distribution from a priori information. The forward model runs with this initial estimate to obtain the distribution of voltages in the subsurface. The root-mean-square (RMS) error is calculated between the measured voltage and the calculated voltage.
3. Based on the degree of match between simulated and measured voltage, the initial estimate of resistivity is changed and the forward model is rerun. The iterative method is linearizing a highly non-linear problem using Newton's method. Essentially, the program solves the linearized problem to obtain the change in modeled resistivity (Δm) for the next iteration.
4. The resistivity model is updated using the general formula $m_{i+1} = m_i + \Delta m$, where m_{i+1} is the resistivity in a model cell at the next iteration, and the m_i is the current value.
5. Steps 3 and 4 are repeated until the RMS error changes between successive iterations is less than 10%.

The iterative nature of resistivity inversion is necessary, since Eq. 3 is non-linear. The advantage of using the inverted resistivity over the apparent resistivity is a distribution range of resistivity values that are more amenable to a direct quantitative comparison to the natural geologic or hydrologic feature. A more complete discussion of

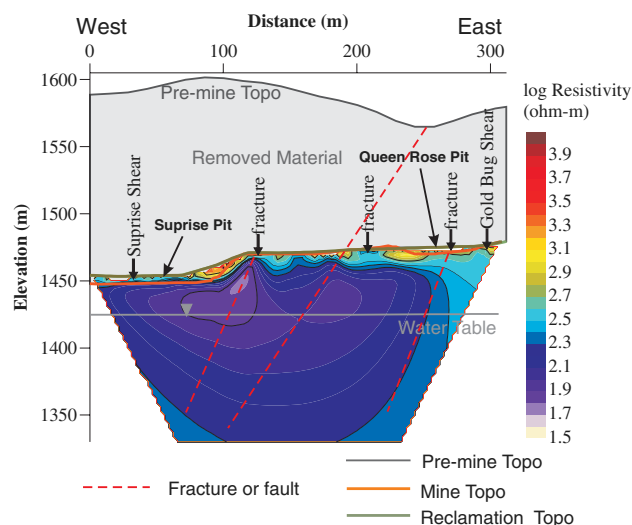


Fig. 4 Resistivity line 0 presented as an example resistivity cross-section showing low resistivity features correlating with pit locations. Faults are interpreted from shapes in resistivity contouring and geologic mapping

resistivity inversion and the methods by which the true resistivity is calculated can be found in several sources, including LaBrecque et al. (1996), Li and Oldenburg (1994), and Loke and Barker (1996).

Methodology

A set of 15 electrical resistivity lines were acquired over the Landusky Mine site. Figure 2 shows the line layout relative to Swift Gulch. The lines were acquired in orthogonal directions, with 12 lines oriented approximately west to east, and three lines oriented approximately north to south. A few lines (lines 1–4) were split due to the steep topography; the pit walls of the Surprise pit presented insurmountable challenges for data acquisition. Four of the lines were acquired between the mine and Swift Gulch in heavily wooded areas.

The electrical resistivity data were acquired with an AGI SuperSting R8 (Advanced Geosciences, Inc., Austin, Texas) resistivity instrument with an 84 channel multiplexer and associated cabling. A pole–pole resistivity array was used with an electrode interval of 3 m. The Tx remote electrode was installed 1,200 m southwest and the Rx remote electrode was installed 1,700 m southeast of the project area. The lengths of the lines ranged from 216 to 585 m and a total of 6,563 m of lineal coverage was completed.

Electrical resistivity completed strictly from the surface of the earth will produce good data near the surface, but has reduced sensitivity with depth (Oldenburg and Li 1999). Data acquired from wells and seeps can help increase the sensitivity of the method. In addition to the electrodes on

the surface, nine wells (ZL-204, ZL-313, ZL-314, ZL-315, ZL-401, ZL-402, ZL-403, ZL-404, and ZL-405) and four seeps along Swift Gulch were each instrumented with a single transmission electrode in contact with ground water (up to 100 m below ground surface). Figure 2 shows the location of the wells and seeps. The resistivity data from these were useful in the three dimensional modeling because they provided valuable insight to what was occurring at depth and at the outflow of ARD along the gulch.

The data were processed in both 2D (as profile sections) and 3D (for volumetric calculations). For 2D, the code EarthImager2D v.2.3.2 (AGI, Austin, TX) was used on a Dell Precision M6300 laptop computer with 2 GB of RAM. Each inversion took less than five minutes to complete. For 3D, the multi-processor code, EarthImager3DCL v1.1.3 (AGI, Austin, TX) was used to invert the data. Three-dimensional numerical inverse modeling of resistivity data is computer memory and processor intensive (Rucker et al. 2009), requiring large computer systems to successfully model the data. For this application, the processing system consisted of a Dell PowerEdge 6800 running a Microsoft Windows Server 2003 ×64 with four dual core Intel Xeon 7120M processors (3 GHz) and 32 GB of RAM.

The dataset used for the resistivity inverse modeling included the resistivity lines as well as the data measured from the nine wells and four seeps. The final data count that was entered into the 3D model was 62,838, using 1,967 electrode locations. Other model parameters include an average resistivity starting model, maximum possible resistivity of 10,000 ohm-m and minimum resistivity of 1 ohm-m. Several 3D models were tested by varying other parameters to ensure the consistency in the results. Each model took approximately 14 days to complete, with a final RMS error less than 7% for each model trial.

Results

An example of the resistivity data acquired at Landusky is shown in Fig. 4, which represents the southernmost line (Line 0). The resistivity data acquisition at Landusky was along transects, and initial evaluation of the data was conducted by examining the individual profiles of each line. The profiles of resistivity data were inverted in 2D and the resistivity values are presented as log transformed. The inverse model finished within three iterations and a final root mean square error of 4.78%. The eastern portion of Line 0 extends across the Queen Rose Pit, while the western portion descends over the Surprise Pit wall, and into the bottom of the Surprise Pit. The distribution of resistivity values within Line 0 is generally uniform, dominated by

values between 50 ($\log_{10}50 = 1.7$) and 300 ($\log_{10}300 = 2.48$) ohm-m. The areas of lowest resistivity appear to correspond with the eastern edge of the Surprise Pit wall. The highest values are nearer the surface, and likely represent competent desiccated rock or reclamation cover material. The water table information was taken from the piezometric surface of Fig. 2.

The fracture and shear locations from Fig. 2, indicated with a black arrow along the top of Line 0, were taken from the regional geologic map. They were used for comparison with interpreted features in the resistivity section. Generally, faulting and fracturing strikes to the northeast and dips steeply towards the northwest. Richardson (1973) also discussed this type of structure in his geologic interpretation of the area. Based on the pattern of the resistivity contours, a number of interpreted fractures have been superimposed on the resistivity section. The most important fracture appears to be at the location of lowest resistivity, just east of the Surprise pit. For reference, the pre-mine topography is displayed atop the Line 0 section, showing the amount of material removed during open pit mining. The pre-mining topographical low at around 250 m is likely the result of localized faulting. A line drawn from this low point and dipping to the northwest correlates with a fracture/fault indicated in the geologic map. The fault is interpreted in the resistivity contouring based on the split in the high angle contouring line along the western edge of the resistivity body (east of the fault). All of the other resistivity lines that ran perpendicular to the high angle faulting exhibited similar behavior.

Fractures, faults, and fissure mapping with geophysics is fairly common, and have been presented in a number of separate studies. The main component to finding these structural features is the offset in contouring or a large change in resistivity values along lineations consistent with separate geologic mapping. Janssen et al. (2002) used magnetotellurics (MT) to map the electrical resistivity of a faulted system in Chile. Mogi et al. (1991) also used MT in Japan to map faults. At the scale of measurement that these studies were conducted, MT is a better choice than an electrical resistivity survey. However, both electrical resistivity imaging and MT give the same quantitative intrinsic property of electrical resistivity. On more local scales, the edge of the Eumsung Basin in Korea was successfully imaged in terms of surface location of the fault zones and delineation of the basin architecture using electrical resistivity (Kim et al. 2001). More recently, Nguyen et al. (2007) demonstrated how inversion of electrical resistivity profiles was applied along the Trévaresse reverse fault (Provence, SE France) to detect shallow deformation patterns. Imaging faulting patterns in the Landusky dataset is consistent with previous analyses.

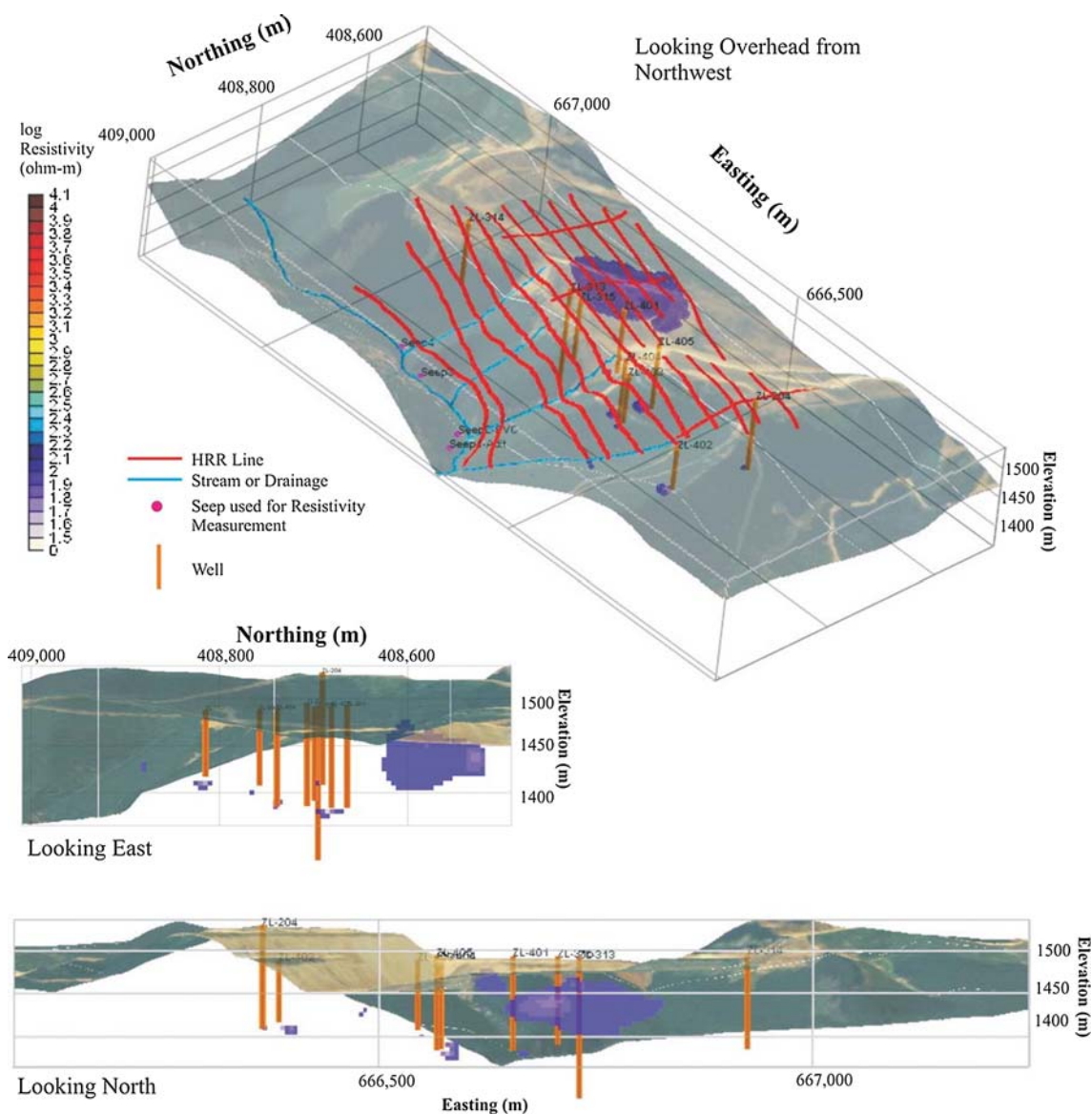


Fig. 5 Three dimensional resistivity of the northern portion of the Landusky Mine, including the Swift Gulch region. The focus of plot is on the lowest (<100 ohm-m) resistivity

To obtain a coherent rendering of the subsurface that adheres to all electrical data, a 3D inversion model was created. The inversion builds up a three dimensional spatial representation of electrical properties that allows a direct interpretation of subsurface features across multiple lines. The major disadvantages of 3D inversion is that much more data are needed to successfully model the subsurface, and more time is required to process the data.

The results of the 3D processing are shown in Figs. 5 and 6. The data are presented as solid rendered bodies at a constant resistivity level (or isopach). The process of viewing the resistivity data can be likened to an onion, where the outermost layers of the onion were peeled away, leaving the core for viewing. Figure 5 reveals the lowest

resistivity values (<100 ohm-m), which are located beneath the pits. Three views of the resistivity are presented, including a 3D view from overhead and two side views looking north and east. Figure 6 shows a slightly elevated resistivity isopach (400 ohm-m) presented in a similar fashion. The higher resistivity shows a larger encompassed volume, which could be coincident with the saturated sediments below the water table. The figure also shows some low resistivity “fingers” that extend along some of the known drainages to Swift Gulch. The lower resistivity body highlighted in Fig. 5 focuses on the potential source of these higher resistivity fingers, which is coincident with the historical pit area. Furthermore, the drainages are thought to be extensions of mapped faults

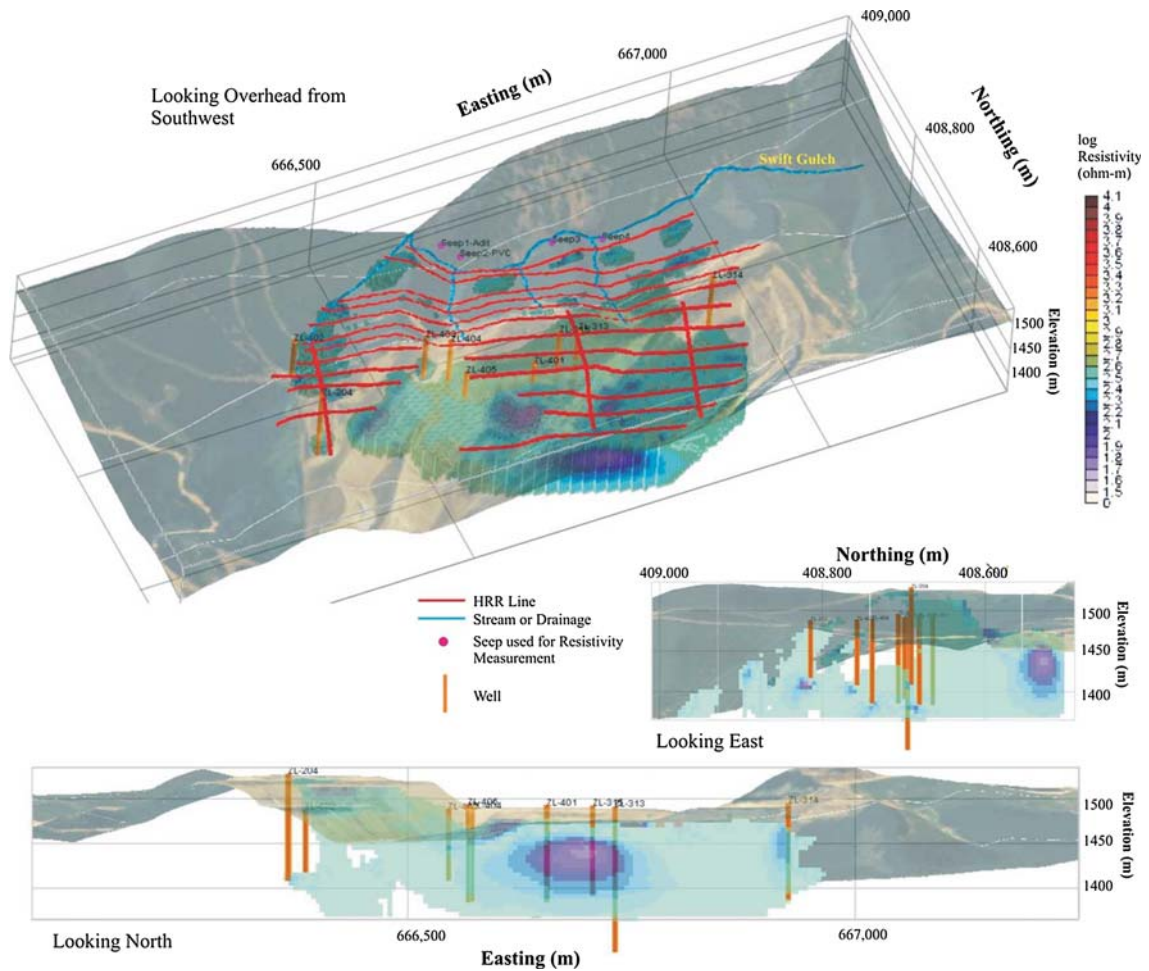


Fig. 6 Three dimensional resistivity of the northern portion of the Landusky Mine, including the Swift Gulch region. The focus of plot is on the lowest (<400 ohm-m) resistivity

Fig. 7 Overhead view of three resistivity isopleths values: 80, 200, and 400 ohm-m; TDS (mg/L) from ground water sampling is also shown

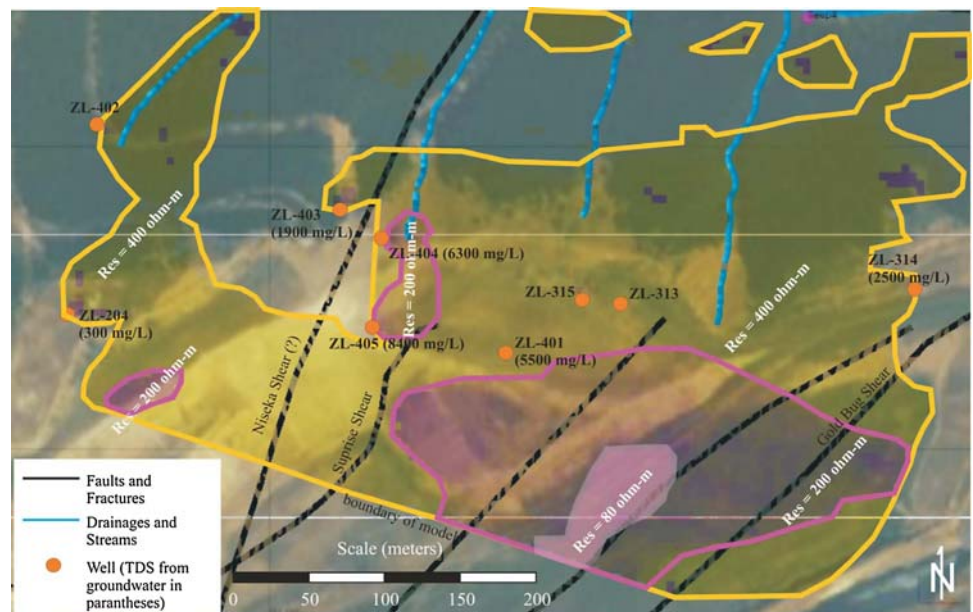
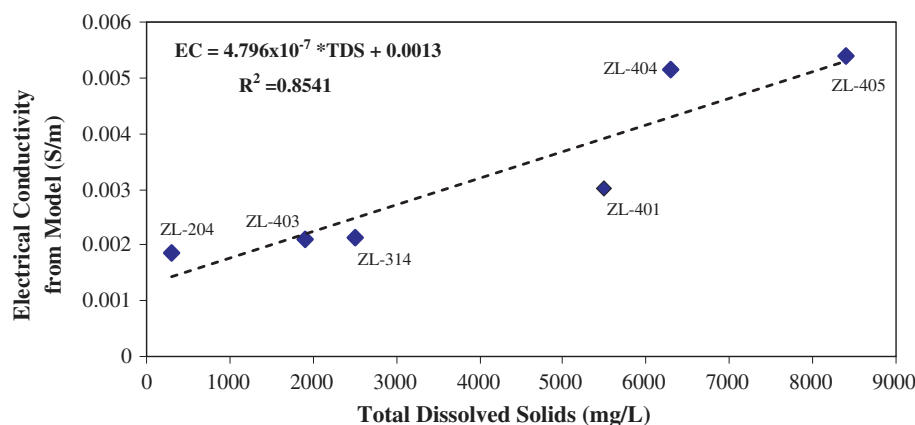


Fig. 8 Linear regression model between electrical resistivity from 3D modeling (presented as electrical conductivity in S/m) and TDS (mg/L)



and their impacts can be seen in the individual resistivity profiles. Although not shown, the largest resistivity values (upwards to 10,000 ohm-m) are typically contained within the upper portions of the model.

Figure 7 shows an overhead view and an outline of several resistivity isopach values, including 80, 200, and 400 ohm-m. The 400 ohm-m body encompasses much of the mine region and along a couple of drainages. The lower resistivity body of 200 ohm-m can be seen mostly at the pit, but also includes a few isolated areas around wells ZL-404 and ZL-405 and southeast of ZL-204. From the figure, it is obvious that the lowest value of 80 ohm-m trends northeast along the western edge of a mapped fault. The feature extends across several individual resistivity lines and its continuity in the three dimensional inversion is consistent with the profile data. The elongated shape of the 80 ohm-m resistivity body in conjunction with its proximity to the pits and faults is strong evidence of possible ARD movement along the fracture system. However, an alternative hypothesis is that the resistivity is imaging the epithermal mineralization hosted in the fractures. Given that the 80 ohm-m low resistivity body is oriented along the same strike as the mineralization, it is reasonable to suspect that the sulfide and iron ions of the pyrite may be responsible for all or part of the anomaly.

To help explain some of the intensity of the resistivity anomalies, the TDS data (taken from Fig. 2) is presented for many of the wells in Fig. 7. The TDS indicates the ionic strength of the pore water, with higher TDS exhibiting lower electrical resistivity values. Interestingly, the wells ZL-404 and ZL-405 show high TDS (6,300 mg/L and 8,400 mg/L) and are within the 200 ohm-m body. Well ZL-401 has a TDS of 5,500 mg/L and is very near the 200 ohm-m body. Quantitatively, this is shown in Fig. 8 as a scatter of bulk electrical conductivity (reciprocal of electrical resistivity) versus TDS. There is a strong correlation between the two variables ($R^2 = 0.85$). Others have shown similar responses of bulk electrical conductivity from geophysical measurements to ground water samples

(e.g. Atekwana et al. 2004; Slater and Glaser 2003). If the linear regression formula can be extrapolated with reasonable fidelity, then one could expect a TDS value of at least 23,000 mg/L within the bounds outlined by the 80 ohm-m contour.

Singha and Gorelick (2006) have noted, however, that “statistical correlation built between colocated fluid and estimated bulk-media electrical conductivities at a particular location would not necessarily be appropriate elsewhere [in the model] or even at the same location at another time”, making the extrapolation of the regression in Fig. 8 highly suspect. Yet, regardless of the validity of Fig. 8 to other unsampled sites, it does lend strong credence to the hypothesis that the surface resistivity measurements are imaging relative changes in ARD concentration in ground water across the site and not simply differences in mineralization due to the epithermal mineral deposits. Many have used electrical resistivity to map contaminated ground water, such as at landfills (Bernstone et al. 2000; Lima et al. 1995; Mota et al. 2004; Perozzi and Holliger 2008), locations affected by salt water intrusion (Nowroozi et al. 1999), degradation of hydrocarbons (Atekwana et al. 2000), and nitrate loading from irrigation (Boadu et al. 2008; Casas et al. 2008). Regardless of application, the addition of water with higher ionic strength than the natural water likely will affect the electrical resistivity. ARD definitely falls within this scope.

Conclusions

A geophysical survey in the form of electrical resistivity was conducted at the Landusky mine site. The technique was summarily applied along parallel and orthogonal transects to build up an image of electrical properties of the subsurface. A total of 15 resistivity lines were acquired over the site using the pole–pole array. Additionally, wells and seeps were used to provide extra sensitivity of the method deeper within the earth. The large dataset from

both surface lines and wells/seeps provided an opportunity to process the data with a true 3D numerical inversion model. The inversion model was constructed by properly geo-referencing the electrode and well locations. The final inverted resistivity data were interpreted by evaluating the intensity of the low resistivity features as well as the shape of the resistivity contours.

The results of the 3D inversion model shows how the lowest resistivity feature appears on the western edge of the Queen Rose pit, coincident with a mapped fracture. The low resistivity feature trends to the northeast, similar to other structural features of the site. The shape, orientation, and truncation of the 80 ohm-m contour at the edge of the pit in Fig. 7 lends some credence to a hypothesis that ARD may be seeping along the fractures towards Swift Gulch.

An overlay of ground water data on the 3D resistivity model shows a correlation of low resistivity and high total dissolved solids (TDS). Wells ZL-404 and ZL-405 measured the highest TDS (both greater than 6,300 mg/L) and correlated well with the 200 ohm-m contour. Well ZL-401 with a TDS of 5,500 mg/L plotted very near the 200 ohm-m contour, and wells ZL-314 and ZL-403, with TDS values of 1,800 and 2,500 mg/L, respectively, plotted on the edge of the 400 ohm-m contour. Figure 8 presents a linear regression model using the reciprocal of resistivity (electrical conductivity) versus TDS. The regression model confirms a strong correlation, which can be used to convert the modeled resistivity to an estimated TDS value. If the model can be extrapolated beyond the bounds of the measured data, then the 80 ohm-m resistivity contours encountered at the pit should produce TDS values near 23,000 mg/L.

Acknowledgments The work was funded by the Montana Department of Environmental Quality (DEQ), Department of Natural Resources and Conservation, U.S. Bureau of Land Management, and a Montana legislative grant under DEQ contract # 506067. Special thanks to Seth Gering for creating Figures 1 and 2. Additional thanks to Michael McNeill, Jason Greenwood, Ryan Brauchla, and Brian Cabbage for acquiring the resistivity data.

References

Atekwana E, Sauck W, Werkema D (2000) Investigations of geoelectrical signatures at a hydrocarbon contaminated site. *J Appl Geophys* 44:167–180

Atekwana E, Atekwana E, Rowe R, Werkema D, Legall F (2004) The relationship of total dissolved solids measurements to bulk electrical conductivity in an aquifer contaminated with hydrocarbon. *J Appl Geophys* 56:281–294

Bayer P, Finkel M (2006) Life cycle assessment of active and passive ground water remediation technologies. *J Contam Hydrol* 83:171–199

Bernstone C, Dahlin T, Ohlsson T, Hogland W (2000) DC-resistivity mapping of internal landfill structures: two pre-excavation surveys. *Environ Geol* 39:360–371

Bird D (2003) Characterization of anthropogenic and natural sources of acid rock drainage at the Cinnamon Gulch abandoned mine land inventory site, Summit County, Colorado. *Environ Geol* 44(8):919–932

Boadu F, Owusu-Nimo F, Menyeh A (2008) Nitrate contamination in ground water at farmlands in Nsawam, Ghana: the role of fractures from azimuthal resistivity surveys. *Environ Eng Geophys* 13:27–32

Brown J, Bassett R, Glynn P (1998) Analysis and simulation of reactive transport in ground water in Pinal Creek Basin, Arizona. *J Hydrol* 209:225–250

Casas A, Himi M, Diaz Y, Pinto V, Font X, Tapias J (2008) Assessing aquifer vulnerability to pollutants by electrical resistivity tomography (ERT) at a nitrate vulnerable zone in NE Spain. *Environ Geol* 54:515–520

Da Silva E, Fonseca E, Matos J, Patinha C, Reis P, Santos O (2005) The effect of unconfined mine tailings on the geochemistry of soils, sediments and surface waters of the Lousal area. *Land Degrad Dev* 16(2):213–228

Damigos D (2006) An overview of environmental valuation methods for the mining industry. *J Clean Prod* 14:234–247

Ebraheem A, Hamburger M, Bayless E, Krothe N (1990) A study of acid mine drainage using earth resistivity measurements. *Ground Water* 28:361–368

El Khalil H, El Hamiani O, Bitton G, Ouazzani N, Boularbah A (2008) Heavy metal contamination from mining sites in South Morocco: monitoring metal content and toxicity of soil runoff and ground water. *Environ Monit Assess* 136:147–160

Finlayson B, Fujimura R, Huang Z (2000) Toxicity of metal-contaminated sediments from Keswick Reservoir, California, USA. *Environ Toxicol Chem* 19(2):485–494

Fischer P, Sexauer G (2002) Influence of natural sources on mercury in water, sediment and aquatic biota in seven tributary streams of the East Fork of the Upper Carson River, California. *Water Air Soil Pollut* 133(1–4):283–295

Hastings J (1988) Gold deposits of Zortman-Landusky, Little Rocky Mountains, Montana. In: Schafer R, Cooper J, Vikre P (eds) 1988 Bulk mineable precious metal deposits of the western United States. Geological Society of Nevada, Reno, pp 187–205

Hazen J, Williams M, Stover B, Wireman M (2002) Characterization of acid mine drainage using a combination of hydrometric, chemical and isotopic analyses, Mary Murphy Mine, Colorado. *Environ Geochem Health* 24:1–22

Janssen C, Hoffmann-Rothe A, Tauber S, Wilke H (2002) Internal structure of the Precordilleran fault system (Chile) – insights from structural and geophysical observations. *J Struct Geol* 24:123–143

Johnson R (2007) Ground water flow modeling with sensitivity analyses to guide field data collection in a mountain watershed. *Ground Water Monit Rev* 27(1):75–83

Kim J, Han S, Ryang W (2001) On the use of statistical methods to interpret electrical resistivity data from the Eumsung basin (Cretaceous), Korea. *J Appl Geophys* 48:199–217

Knechtel M (1959) Stratigraphy of the Little Rocky Mountains and encircling foothills, Montana. *USGS Bull* 1072-N:723–749

LaBrecque D, Miletto M, Daily W (1996) The effects of noise on Occam's inversion of resistivity tomography data. *Geophysics* 61(2):538–548

Li Y, Oldenburg D (1994) Inversion of 3-D DC resistivity data using an approximate inverse mapping. *Geophys J Int* 116:527–537

Lima O, Sato H, Porsani M (1995) Imaging industrial contaminant plumes with resistivity techniques. *J Appl Geophys* 34:93–108

Liu W, Coveney R, Chen J (2003) Environmental quality assessment on a river system polluted by mining activities. *Appl Geochem* 18(5):749–764

- Loke M, Barker R (1996) Rapid least-squares inversion of apparent resistivity pseudosections by a quasi-Newton method. *Geophys Prospect* 44(1):131–152
- Malmstrom M, Berglund S, Jarsjo J (2008) Combined effects of spatially variable flow and mineralogy on the attenuation of acid mine drainage in ground water. *Appl Geochem* 23(6):1419–1436
- Merkel R (1972) The use of resistivity techniques to delineate acid mine drainage in ground water. *Ground Water* 10:38–42
- Mian M, Yanful E (2003) Tailings erosion and resuspension in two mine tailings ponds due to wind waves. *Adv Environ Res* 7:745–765
- Mogi T, Katsura I, Nishimura S (1991) Magnetotelluric survey of an active fault system in the northern part of Kinki District, southwest Japan. *J Struct Geol* 13:235–240
- Mota R, Monteiro Santos F, Mateus A, Marques F, Gonçalves M, Figueiras J, Amaral H (2004) Granite fracturing and incipient pollution beneath a recent landfill facility as detected by geoelectrical surveys. *J Appl Geophys* 57:11–22
- Nguyen F, Garambois S, Chardon D, Hermitte D, Bellier O, Jongmans D (2007) Subsurface electrical imaging of anisotropic formations affected by a slow active reverse fault, Provence, France. *J Appl Geophys* 62:338–353
- Nowroozi A, Horrocks S, Henderson P (1999) Saltwater intrusion into the freshwater aquifer in the eastern shore of Virginia: a reconnaissance electrical resistivity survey. *J Appl Geophys* 42:1–22
- Oldenburg D, Li Y (1999) Estimating depth of investigation in DC resistivity and IP surveys. *Geophysics* 64:403–416
- Osborne T, Adams J, Jepson W (2006) Ground water flow in fractured rock at the Landusky Mine Site, Phillips County, Montana. Abstracts, annual meeting of the American Water Resources Association, Montana Section, Polson, MT, USA
- Parker S, Gammons C, Jones C, Nimick D (2007) Role of hydrous iron oxide formation in attenuation and diel cycling of dissolved trace metals in a stream affected by acid rock drainage. *Water Air Soil Pollut* 181:247–263
- Passariello B, Giuliano V, Quaresima S, Barbaro M, Caroli S, Forte G, Carelli G, Iavicoli I (2002) Evaluation of environmental contamination at an abandoned mining site. *Microchem J* 73:245–250
- Perozzi L, Holliger K (2008) Detection and characterization of preferential flow paths in the downstream area of a hazardous landfill. *J Environ Eng Geophys* 13:343–350
- Richardson G (1973) Geology and ore deposits of the Landusky Mining District, Phillips County, Montana. MS Thesis, University of Arizona, Tucson, AZ, USA
- Robain H, Albouy Y, Dabas M et al (1999) The location of infinite electrodes in pole-pole electrical surveys: consequences for 2D imaging. *J Appl Geophys* 41:313–333
- Roy A, Apparao A (1971) Depth of investigation in direct current methods. *Geophysics* 36:943–959
- Rucker D, Fink J (2007) Inorganic plume delineation using surface high resolution electrical resistivity at the BC Cribs and Trenches Site, Hanford. *Vadose Zone J* 6:946–958
- Rucker D, Levitt M, Greenwood J (2009) Three-dimensional electrical resistivity model of a nuclear waste disposal site. *J Appl Geophys* (in press)
- Saiki M, Martin B, Thompson L, Welsh D (2001) Copper, cadmium, and zinc concentrations in Juvenile chinook salmon and selected fish-forage organisms (aquatic insects) in the upper Sacramento River, California. *Water Air Soil Pollut* 132:127–139
- Salomons W (1995) Environmental impact of metals derived from mining activities: processes, predictions, prevention. *J Geochem Explor* 52:5–23
- Shaw S, Robertson A, Maehl W (2000) Material characterization and prioritization of remediation measures at the Zortman/Landusky mine sites. Proceedings of 2000 Billings land reclamation symposium, Billings, Montana, USA, pp 346–358
- Shaw S, Robertson A, Maehl W, Kuipers J, Haight S (2001) Review of the multiple accounts analysis alternatives evaluation process completed for the reclamation of the Zortman/Landusky mine sites. Proceedings of National Association of Abandoned Mine Lands Conference, Athens, Ohio, USA
- Singha K, Gorelick S (2006) Effects of spatially variable resolution on field-scale estimates of tracer concentration from electrical inversions using Archie's law. *Geophysics* 71:G83–G91
- Slater L, Glaser D (2003) Controls on induced polarization in sandy unconsolidated sediments and application to aquifer characterization. *Geophysics* 68:1547
- Spectrum Engineering (2009) Engineering evaluation/cost analysis for water management at the Zortman and Landusky Mines, Phillips County, Montana. Prepared for the US Bureau of Land Management, http://www.blm.gov/mt/st/en/fo/lewistown_field_office/zortman.html
- Spindler K, Olyphant G (2004) Geophysical investigations at an abandoned mine site subjected to reclamation using a fixated scrubber sludge cap. *Environ Eng Geosci* 10:243–251
- Telford W, Geldart L, Sheriff R (1990) Applied geophysics. Cambridge University Press, Cambridge, UK, p 790
- Warhurst A, Mitchell P (2000) Corporate social responsibility and the case of Summitville mine. *Res Policy* 26:91–102
- Wilson M, Kyser T (1988) Geochemistry of porphyry-hosted Au-Ag deposits in the Little Rocky Mountains, Montana. *Econ Geol* 83:1329–1346
- Yuval D, Oldenburg W (1996) DC resistivity and IP methods in acid mine drainage problems: results from the Copper Cliff mine tailings impoundments. *J Appl Geophys* 34:187–198